Prediction of giant anomalous Nernst Effect in $Sm(Co,Ni)_5$

Naoki Chiba[1,2], Keisuke Masuda[1], Ken-ichi Uchida[1,2], and Yoshio Miura[1,3,4,a)*]

AFFILIATIONS

[1] Research Center for Magnetic and Spintronic Materials, National Institute for Materials Science, Tsukuba 305-0047, Japan

[2] Department of Mechanical Engineering, The University of Tokyo, Tokyo 113-8656, Japan

[3] Faculty of Electrical Engineering and Electronics, Kyoto Institute of Technology, Kyoto 606-8585, Japan

[4] Center for Spintronics Research Network, Osaka University, Osaka 560-8531, Japan

[a)] Author to whom correspondence should be addressed: MIURA.Yoshio@nims.go.jp

ABSTRACT

Sm-Co bulk alloys are well known permanent magnets having large remanent magnetizations and coercive forces and are widely used in many industrial products. Recently, a large transverse thermoelectric conversion was observed for $SmCo_5$ over a wide temperature range in the absence of magnetic fields. The large anomalous Nernst coefficient (ANC) was also confirmed by the first-principles density functional theory (DFT) calculations. In this study, we predicted further enhancement of the ANC by including Ni in Co site of $SmCo_5$. We showed that the ANC of $Sm(Co_{1-x}Ni_x)_5$ increases with increasing the Ni ratio and takes the maximum value α_{xy} = 11.3 A K^{-1} m^{-1} around x = 0.08 at 300 K, which is about 77% enhancement of α_{xy} = 6.4 A K^{-1} m^{-1} in $SmCo_5$. We clarified that the band-proximity points near the nodal line of $Sm(Co_{0.92}Ni_{0.08})_5$ are the main contributing factor to the large Berry curvature, providing the steep slope of the energy dependence in the anomalous Hall conductivity around the Fermi energy.

Thermoelectric generation is based on the conversion of heat into electricity driven by the Seebeck effect,[1] which can be applied to stand-alone power sources for IoT devices and the reuse of waste heat.[2,3] However, there are some issues that prevent the technology from widely being used because of the complexity of the three-dimensional structure of the integrated elements in the device and the inclusions of rare and toxic elements in the materials that show excellent thermoelectric conversion performance.[4,5] On the other hand, transverse thermoelectric conversion by the anomalous Nernst effect (ANE) has attracted much attention in recent years.[6-8] The ANE is a thermoelectric effect unique to magnetic materials and generates an electric filed in the direction perpendicular to the temperature gradient and the magnetization.[9-12] This means that the electric voltage generated by ANE can be increased simply by increasing the length of the device plane perpendicular to the temperature gradient.[6,7] However, compared to Seebeck-type thermoelectric conversion, the thermoelectric capacity is significantly insufficient, and the search for new materials is strongly required.

To enhance the thermoelectric performance of ANE, we need materials with large anomalous Nernst coefficient S_{ANE}, which is expressed as[7]

$$S_{\mathrm{ANE}} = \rho_{xx}\alpha_{xy} + \rho_{xy}\alpha_{xx}. \quad (1)$$

ρ_{xx} (ρ_{xy}) and α_{xx} (α_{xy}) are the diagonal (off diagonal) components of the electric resistivity and thermoelectric conductivity tensors, respectively. The first term of Eq. (1) originates from the transverse thermoelectric conductivity α_{xy} and is regarded as an intrinsic part of ANE. The second term is attributed to a contribution of the longitudinal thermopower i.e., the Seebeck effect, which is usually smaller than the first term due to small anomalous Hall angle (ρ_{xy}/ρ_{xx}) and/or Seebeck coefficient. Thus, the material design with large α_{xy} will be required to enhance S_{ANE}. Recently, large S_{ANE} were observed in ferromagnetic Heusler compound Co_2MnGa[13,14] and $Co_2MnAl_{1-x}Si_x$,[15] which can be attributed to the large α_{xy} due to the topological nature of the band dispersion.

Recent studies have indicated that multilayered superlattice is effective in increasing the ANE. Various magnetic/nonmagnetic combinations in multilayer systems show an increase in ANE by varying parameters such as the number of layers and the number of stacks.[16-18]

Seki, *et al.*, demonstrated the enhancement of ANE owing to the formation of Ni/Pt superlattices. They found an optimized transverse thermoelectric conductivity, reaching $\alpha_{xy} = 4.8$ A K^{-1} m^{-1} for thickness of Ni layer $t = 4.0$ nm, which was the remarkable enhancement compared to the bulk Ni.[18] Furthermore, in our recent study, we demonstrated an effectiveness of multilayer formation to obtain larger α_{xy} for Co/Ni multilayer system based on Bayesian optimization and first-principles calculations.[19] We clarified that the multilayer formation with one monolayer alloying Co and Ni causes a fine modulation in band structure and the proximity of bands with different states of parity near the Fermi energy. Such band modulation can enhance $|\alpha_{xy}|$ up to ~10 A K^{-1} m^{-1}, indicating an effectiveness of the multilayer formation.

Another recently reported system which shows relatively large α_{xy} is permanent magnets. It was found that the well-known rare-earth $SmCo_5$ permanent magnets show the anomalous Nernst coefficient $|S_{\mathrm{ANE}}|$ ~5 μV K^{-1} at >400 K.[20] The $|\alpha_{xy}|$ of $SmCo_5$ is more than one order of magnitude greater than those for typical ferromagnetic metals and the figure of merit *ZT* above room temperature is comparable to that in Co_2MnGa.[13,14] Furthermore, the S_{ANE} of the $SmCo_5$ magnets monotonically increases with increasing the temperature and shows the highest value of *ZT* reported so far at $T > 500$ K.[21] We calculated the α_{xy} of $SmCo_5$ by the linear response theory combined with the first-principles calculations including the orbital polarization correction and obtained relatively large α_{xy} corresponding to 6 A K^{-1} m^{-1} at the Fermi level.[20] The calculations suggest that α_{xy} of $SmCo_5$ has a maximum value not at the Fermi energy but at the chemical potential μ = 0.04 eV.[20] These results indicate that the substitution effect is also important in enhancing α_{xy} of $SmCo_5$-type permanent magnets.

Since permanent magnets are widely used in a society, the addition of thermoelectric conversion functionality will contribute to the development of various energy-harvesting technologies. Furthermore, $SmCo_5$-type permanent magnets have large remanent magnetization and coercive force, stable transverse thermoelectric conversion can be realized over a wide temperature range in the absence of magnetic fields.[22] In this work, we theoretically investigate and discuss the enhancement of α_{xy} of $SmCo_5$-type permanent magnets. Here, we focus on the intrinsic part of ANE, especially the transverse thermoelectric conductivity α_{xy}, because the previous experiments indicated that the large AEE and ANE of $SmCo_5$ originated from the intrinsic properties of α_{xy} in a wide

temperature range.[20,21] Since Ni-doped $SmCo_5$ has never been synthesized in experiments, it is very important for future studies to experimentally investigate not only the intrinsic effects but also the extrinsic effects.[23] We mainly discuss the dependence of α_{xy} on substituting Ni for Co of $SmCo_5$ because our previous study indicates the importance in controlling the Fermi level of $SmCo_5$ to enhance α_{xy}.[20] We found that the substitution of Ni for Co of $SmCo_5$ can enhance α_{xy} more than 10 A K^{-1} m^{-1}.

The transverse transport coefficients of $Sm(Co_{1-x}Ni_x)_5$ were calculated by the linear response theory[24,25] combined with the first-principles calculations. We calculated the electronic structures and the matrix elements of momentum operator of $Sm(Co_{1-x}Ni_x)_5$ by means of the full-potential linearized augmented plane wave method (FLAPW) including the full-relativistic effect, which is implemented in the WIEN2k code.[26] The generalized gradient approximation proposed by Perdew, Burke, and Ernzerhof was adopted for the exchange and correlation energies.[27] We used the virtual crystal approximation[28] (VCA) for Co-Ni disordering in $SmCo_5$. Here, we considered a homogeneous doping of Ni in Co site of $SmCo_5$ because we used the VCA for Co-Ni disordering. The VCA has been applied to the calculation of α_{xy} in previous studies,[29] where a dopant concentration dependence of α_{xy} by VCA shows a good agreement with experimental results, indicating the effectiveness of VCA in transverse transport coefficients.

The atomic structure of $SmCo_5$ with the hexagonal unit cell is shown in the left-upper inset in Fig. 1. The lattice constant of the primitive unit cell of $SmCo_5$ ($SmNi_5$) was fixed to a = 4.982 (4.926) Å and c = 3.975 (3.980) Å. Then, we set the lattice constant of $Sm(Co_{1-x}Ni_x)_5$ according to the Vegard's rule, where the atomic positions are fixed at each lattice constant. In the calculation, we considered the orbital polarization effect in the spin-orbit Hamiltonian in order to satisfy the Hund rule in *f*-orbitals of Sm atom, where the additional potential having the form $V_{\mathrm{op}} = c_{\mathrm{op}}\langle L_z\rangle l_z$ was added to the system.[30-32] Here, c_{op} is the orbital polarization parameter, $\langle L_z\rangle$ is projection of the orbital momentum on the magnetization direction **M,** and l_z is single electron orbital momentum component *z* parallel to **M**. Then, we considered the on-site Coulomb interaction U and the Hund coupling J for *f*-orbitals of Sm and *d*-orbitals of Ni atoms because of the strong electron correlation[33,34]. Here, we chose U =9.00 eV and J = 0.75 eV for Sm atom and U = 3.9 eV and J = 1.1 eV for Ni atom which satisfy orbital magnetic moment according to the Hund rule.[35,36] We obtained an anti-

ferromagnetic state for the spin moments between Sm and Co atoms from the self-consistent-field calculation with 19 × 19 × 21 k-points, which is energetically more stable than the ferromagnetic state. We checked the U dependence of the orbital magnetic moment of Sm in $SmCo_5$. We found that the orbital magnetic moments of Sm strongly depend on the U value, which are around 2 μ_B at U = 0.00 eV and 4 μ_B at U = 5.00 eV. On the other hand, it is around 5 μ_B at U = 9.00 eV, which satisfy the second Hund's rule. Once the correct orbital magnetic moment around 5 μ_B according to the second Hund rule for Sm is obtained, the DFT+U calculation gives the reasonable electronic structures within DFT.[35] Thus, we adopted U = 9.00 eV for Sm f orbital, which yields a large α_{xy} around 6 $K^{-1}Am^{-1}$. Another method for dealing localized f orbitals is the Quasiparticle self-consistent GW (QSGW) method.[37] The QSGW method approximately treats quasiparticle states, and thus can correctly calculate the localized and excited states. Compared to the DFT+U calculation, the QSGW calculation generally reduces the bandwidth of d and f states, leading to the enhancement of σ_{xy} and α_{xy} around the Fermi level. Individual discussions on the QSGW calculations for Ni-doped $SmCo_5$ will be future tasks.

Then, we calculated the anomalous Hall conductivity σ_{xy} by following equations,[38,39]

$$\sigma_{xy}(E) = -\frac{e^2}{\hbar}\int \frac{d^3k}{(2\pi)^3}\Omega^z(\mathbf{k},E). \quad (2)$$

$\Omega^z(\mathbf{k},E)$ is the Berry curvature given by

$$\Omega^z(\mathbf{k},E) = 2\sum_{n>m}\Omega^z_{mn}(\mathbf{k},E), \quad (3)$$

$$\Omega^z_{mn}(\mathbf{k},E) = \frac{\hbar^2}{m_e^2}[f_{\mathbf{k}m}(E) - f_{\mathbf{k}n}(E)]\frac{\mathrm{Im}\langle \mathbf{k}m|p_x|\mathbf{k}n\rangle\langle \mathbf{k}n|p_y|\mathbf{k}m\rangle}{(\varepsilon_{\mathbf{k}n} - \varepsilon_{\mathbf{k}m})^2}, \quad (4)$$

where m and n are the occupied and unoccupied band indices, p_x (p_y) is the x (y) component of the momentum operator, $|\mathbf{k}n\rangle$ is the eigenstate with the eigenenergy $\varepsilon_{\mathbf{k}n}$, and $f_{\mathbf{k}n}(E)$ is the occupation function for the band n and wave-vector $\mathbf{k}$ at the energy E relative to the Fermi energy. In the σ_{xy} calculation, the **M** direction was set to be along the c axis of the unit cell, and the uniform k-point mesh of 68 × 68 × 73 was used for the Brillouin-zone (BZ) integration providing good convergence for σ_{xy}. The α_{xy} value at temperature T was obtained from the Boltzmann transport theory by integrating σ_{xy} with energy E,[20]

$$\alpha_{xy} = -\frac{1}{eT}\int dE \left(-\frac{\partial g}{\partial E}\right)(E-\mu)\sigma_{xy}(E)\,, \quad (5)$$

where $g = 1/[\exp((E-\mu)/k_{\mathrm{B}}T) + 1]$ is the Fermi distribution function with the chemical potential μ. The absolute value of α_{xy} for T = 300 K at the Fermi energy, μ = 0 eV, was adopted as the calculation results of α_{xy}.

We show in Fig. 1 total density of states (TDOS) of $Sm(Co_{1-x}Ni_x)_5$ for x = 0.0, 0.1, 0.4, 0.5, and 1.0. In the TDOS of $Sm(Co_{1-x}Ni_x)_5$, we can find several sharp peaks around E - E_F = 3.0, 4.5, and 6.5 eV for the majority-spin state, and E - E_F = -7.5, -6.3, -5.0, 1.5, and 2.0 eV for the minority-spin state. These sharp peaks are due to local density of states (LDOS) of *f*-orbital of Sm, which are well localized far from the Fermi level. Since LDOS around the Fermi level is mainly composed of Co and Ni orbitals in $Sm(Co_{1-x}Ni_x)_5$, the transport properties can also be attributed to electronic states of $Co_{1-x}Ni_x$ sites. The magnifications of the TDOS around the Fermi level are shown in the right-lower inset in Fig. 1. If we focus on the minority-DOS around the Fermi level, we can confirm the rigid band shift of TDOS peaks toward the lower energy regions with increasing x up to x = 0.4 because of one more valence electron of Ni than Co. However, the peaks and their shifts around the Fermi level due to the substitution of Ni for Co disappear and split into two peaks for x = 0.5, indicating that the electronic structures of $Sm(Co_{1-x}Ni_x)_5$ cannot be described by the rigid band model for $x \geq 0.5$.

We show in Figs. 2(a) and (b) the σ_{xy} and α_{xy} values of $Sm(Co_{1-x}Ni_x)_5$ as a function of the Ni ratio x up to x = 0.10, i.e., within the rigid band model. For comparison, the x-dependence of σ_{xy} and α_{xy} values for $Sm(Co_{1-x}Fe_x)_5$ are also shown up to x = 0.10 in Figs. 2(a) and (b). The σ_{xy} values of $Sm(Co_{1-x}Ni_x)_5$ and $Sm(Co_{1-x}Fe_x)_5$ decrease with increasing x due to the Fermi level shift, and the sign changes from plus to minus around x = 0.05 and 0.10, respectively. The α_{xy} value of $Sm(Co_{1-x}Ni_x)_5$ increases with increasing the Ni ratio and reaches the maximum value α_{xy} = 11.3 A K^{-1} m^{-1} around x = 0.08. This value is an improvement of about 77% compared to α_{xy} = 6.4 A K^{-1} m^{-1} in $SmCo_5$. On the other hand, the α_{xy} value of $Sm(Co_{1-x}Fe_x)_5$ decreases with increasing the Fe ratio, clearly indicating the chemical trend of α_{xy} in this system and the importance of Ni substitution for Co. In Fig. 3(a) and (b), the composition dependences of σ_{xy} and α_{xy} are shown for the promising Ni substitution case up to x = 0.4. Here, we calculated σ_{xy} and α_{xy} up to x = 0.4 for $Sm(Co_{1-}$

$_x$Ni$_x$)$_5$, because we do not expect a further increase of the Nernst coefficient in Ni concentration. We confirmed that the Ni substitution for Co enhances the α_{xy} up to $x = 0.14$. The monotonic reduction of α_{xy} by further Ni doping can be attributed to the decrease of Co *d* LDOS by electron doping, because the Co *d* states give the major contribution to the σ_{xy} and α_{xy}. To clarify the origin of the enhancement of α_{xy}, we show in Figs. 3(c) and (d) the energy E dependence of the σ_{xy} and μ dependence of the α_{xy} for x = 0.00 and x = 0.08. Figure 3(c) shows that the large slope of σ_{xy} in SmCo$_5$ is shifted to just above E_F due to Ni substitution for Co. According to the Mott formula obtained from the Sommerfeld expansion of Eq. (5), the absolute value of α_{xy} is proportional to $\partial\sigma_{xy}/\partial E$, i.e., α_{xy} can be attributed to the energy derivative of σ_{xy} at each μ. Therefore, large α_{xy} is obtained for Sm(Co$_{0.92}$Ni$_{0.08}$)$_5$ where the steep slope of $\sigma_{xy}(E)$ is shifted directly above E_F (μ=0) [Figs. 3(c) and (d)]. The comparison of the band dispersion of SmCo$_5$ and Sm(Co$_{0.92}$Ni$_{0.08}$)$_5$ also clarified the shift of the Fermi energy by the Co substitution of SmCo$_5$.

The large α_{xy} (large energy dependence of σ_{xy}) at the Fermi level in Sm(Co$_{0.92}$Ni$_{0.08}$)$_5$ is attributed to the fact that σ_{xy} shows a large positive value (~+1000 S/cm) just below the Fermi level and a large negative value (~ -1000 S/cm) just above the Fermi level. To clarify the origin of the σ_{xy} behavior, the **k**-resolved Berry curvatures of Sm(Co$_{0.92}$Ni$_{0.08}$)$_5$ just below (E - E_F = -0.05 eV) and just above (E - E_F = +0.05 eV) are shown in Fig. 4. In Figs. 4(a) and (b), the Berry curvatures at E - E_F = -0.05 eV and E – E_F = +0.05 eV are mapped onto their iso-energy surfaces of $\varepsilon_{\mathbf{k}n}$ in the BZ. From Fig. 4(a), the large Berry curvature can be confirmed near the lines connecting the L and K high-symmetry points and the H and M high-symmetry points. Figure 4(b) shows a relatively large Berry curvature near the line connecting the L and H points. Figures 4(c) and (d) show the band dispersion just on the high-symmetry lines and the Berry curvatures along the dispersion $\varepsilon_{\mathbf{k}n}$ for E - E_F = $\pm$0.05 eV. The large Berry curvatures are observed on the K-L and M-H high-symmetry lines just below the Fermi level (E – E_F = -0.05 eV) and on the L-H high-symmetry line just above the Fermi level (E – E_F = +0.05 eV), respectively. These behaviors of the Berry curvature in Sm(Co$_{0.92}$Ni$_{0.08}$)$_5$ contribute to the abrupt change in the σ_{xy} near the Fermi level shown in Fig. 4(e).

To obtain more detailed understanding on the origin of σ_{xy}, we focus on the formulation of the Berry curvature given by Eq. (4). The Berry curvature consists of matrix elements of the momentum operator in the numerator and difference between arbitrary eigen-energies in the denominator. Due to the selection rule of dipole transitions, the matrix elements of the momentum operator have non-zero values for transitions between orbital states (*s*, *p*, *d*) with different parity, such as *s*-*p* and *p*-*d* transitions, which depends on the orbital hybridization in occupied and unoccupied eigenstates. On the other hand, the difference of eigen-energies in the denominator reflects the band proximity points, i.e., the so-called nodal-line in the band dispersion, which contributes significantly to the Berry curvature. To estimate the contribution of the nodal line, we calculated the following quantity for $Sm(Co_{0.92}Ni_{0.08})_5$,

$$N(\mathbf{k}, E) = 2 \sum_{n>m} \frac{[f_{\mathbf{k}m}(E) - f_{\mathbf{k}n}(E)]}{(\varepsilon_{\mathbf{k}n} - \varepsilon_{\mathbf{k}m})^2}, \quad (6)$$

which is the sum of Eq. (4) without the matrix elements and contributes to the Berry curvatures around the band proximity points. Figure 4 shows the mapping of the Berry curvature $\Omega^z(\mathbf{k}, E)$ and the nodal line $N(\mathbf{k}, E)$ onto the Fermi surface for three bands crossing the Fermi energy. The plotting Eqs. (4) and (6) on the Fermi surface can show the relationship between the Berry phase and nodal points in the Brillouin zone. For a further understanding, it is necessary to analyze in detail the DOS projected onto the band that creates the nodal line.[40] Comparison of (a) with (d), (b) with (e), and (c) with (f) in Fig. 5 shows that the Berry curvature and nodal line have large peaks in the same region on the Fermi surface in BZ. This suggests that there are many band proximity points in the vicinity of the Fermi energy, which determines the energy dependence of the Berry curvature in $Sm(Co_{0.92}Ni_{0.08})_5$.

In summary, we studied the transverse thermoelectric coefficients of $Sm(Co_{1-x}Ni_x)_5$ based on the linear response theory and the first-principles calculations. We found that α_{xy} of $Sm(Co_{1-x}Ni_x)_5$ increases with increasing the Ni ratio *x* and takes the maximum value α_{xy} = 11.3 A K^{-1} m^{-1} around *x* = 0.08, which is about 77% improvement of α_{xy} = 6.4 A K^{-1} m^{-1} in $SmCo_5$. We clarified that the rigid band shift of electronic structures of $Sm(Co_{1-x}Ni_x)_5$ provides the steep slope of $\sigma_{xy}(E)$ above E_F (μ=0), leading to the large α_{xy} value for $Sm(Co_{0.92}Ni_{0.08})_5$. Furthermore, we revealed that the band proximity points around the nodal line of $Sm(Co_{0.92}Ni_{0.08})_5$ are the main contributing factor to the Berry curvature and the

energy dependence of σ_{xy}. Our results suggest the importance of the tunning of the Fermi level by substituting Ni for Co of $SmCo_5$ for obtaining large transverse thermoelectric coefficients, and experimental verification will be expected.

See the supplementary material for the Ni composition x dependence of spin and orbital magnetic moments of $Sm(Co_{1-x}Ni_x)_5$.

ACKNOWLEDGMENTS

This work was partly supported by Grant-in-Aids for Scientific Research (Grant No. JP22H04966, JP22H04965) from JSPS, CREST "Creation of Innovative Core Technologies for Nano-enabled Thermal Management" (JPMJCR17I1) and ERATO "Magnetic Thermal Management Materials" (JPMJER2201), from JST, Japan.

REFERENCES

[1] H. J. Goldsmid, Introduction to Thermoelectricity (Springer, Berlin, 2009).

[2] L. E. Bell, Science **321**, 1457 (2008).

[3] M. Haras and T. Skotnicki, Nano Energy **54**, 461 (2018).

[4] H. S. Kim, W. Liu, G. Chen, C-W. Chu, and Z. Ren, Proc. Natl. Acad. Sci. **112**, 8205 (2015).

[5] Q. Yan and M. G. Kanatzidis, Nat. Mater. **21**, 503 (2022).

[6] Y. Sakuraba, K. Hasegawa, M. Mizuguchi, T. Kubota, S. Mizukami, T. Miyazaki, and K. Takanashi, Appl. Phys. Exp. **6**, 033003 (2013).

[7] K. Uchida, W. Zhou, and Y. Sakuraba, Appl. Phys. Lett. **118**, 140504 (2021).

[8] K. Uchida and J. P. Heremans, Joule **6**, 2240 (2022).

[9] A. V. Ettingshausen and W. Nernst, Ann. Phys. **265**, 343 (1886).

[10] A. W. Smith, Phys. Rev. **33**, 295 (1911).

[11] P. W. Bridgman, Phys. Rev. **24**, 644 (1924).

[12] E. H. Hall, Phys. Rev. **26**, 820 (1925).

[13] H. Reichlova, R. Schlitz, S. Beckert, P. Swekis, A. Markou, Y. C. Chen, D. Kriegner, S. Fabretti, G. Hyeon Park, A. Niemann, S. Sudheendra, A. Thomas, K. Nielsch, C. Felser, and S. T. B. Goennenwein, Appl. Phys. Lett. **113**, 212405 (2018).

[14] A. Sakai, Y. P. Mizuta, A. A. Nugroho, R. Sihombing, T. Koretsune, M.-T. Suzuki, N. Takemori, R. Ishii, D. Nishio-Hamane, R. Arita, P. Goswami, and S. Nakatsuji, Nat. Phys. **14**, 1119 (2018).
[15] Y. Sakuraba, K. Hyodo, A. Sakuma, and S. Mitani, Phys. Rev. B **101**, 134407 (2020).
[16] K. Uchida, T. Kikkawa, T. Seki, T. Oyake, J. Shiomi, Z. Qiu, K. Takanashi, and E. Saitoh, Phys. Rev. B **92**, 094414 (2015).
[17] C. Fang, C. H. Wan, Z. H. Yuan, L. Huang, X. Zhang, H. Wu, Q. T. Zhang, and X. F. Han, Phys. Rev. B **93**, 054420 (2016).
[18] T. Seki, Y. Sakuraba, K. Masuda, A. Miura, M. Tsujikawa, K. Uchida, T. Kubota, Y. Miura, M. Shirai, and K. Takanashi, Phys. Rev. B **103**, L020402 (2021).
[19] N. Chiba, K. Masuda, K. Uchida, and Y. Miura, APL Mach. Learn. **1**, 026114 (2023).
[20] A. Miura, H. Sepehri-Amin, K. Masuda, H. Tsuchiura, Y. Miura, R. Iguchi, Y. Sakuraba, J. Shiomi, K. Hono, and K. Uchida, Appl. Phys. Lett. **115**, 222403 (2019).
[21] A. Miura, K. Masuda, T. Hirai, R. Iguchi, T. Seki, Y. Miura, H. Tsuchiura, K. Takanashi, and K. Uchida, Appl. Phys. Lett. **117**, 082408 (2020).
[22] K. Takagi, Y. Hirayama, S. Okada, A. Hosokawa, and W. Yamaguchi, KONA Pow. Par. J. **40**, 74 (2023).
[23] S. Onoda, N. Sugimoto, and N. Nagaosa, Phys. Rev. B **77**, 165103 (2008).
[24] H. Nakano, Prog. Theor. Phys. **15**, 77 (1956).
[25] R. Kubo, J. Phys. Soc. Jpn. **12**, 570 (1957).
[26] P. Blaha, K. Schwarz, F. Tran, R. Laskowski, G. K. H. Madsen, and L. D. Marks, J. Chem. Phys. **152**, 074101 (2020).
[27] J. P. Perdew, K. Burke, and M. Ernzerhof, Phys. Rev. Lett. **77**, 3865 (1996).
[28] L. Bellaiche and D. Vanderbilt, Phys. Rev. B **61**, 7877 (2000).
[29] Y. Yanagi, J. Ikeda, K. Fujiwara, K. Nomura, A. Tsukazaki, and M. Suzuki, Phys. Rev. B **103**, 205112 (2021).
[30] O. Eriksson, M. S. S. Brooks, and B. Johansson, Phys. Rev. B **41**, 9087 (1990).
[31] P. Novák, F. Boucher, P. Gressier, P. Blaha, and K. Schwarz, Phys. Rev. B **63**, 235114 (2001).
[32] P. Ravindran, A. Kjekshus, H. Fjellvag, P. James, L. Nordstrom, B. Johansson, and O. Eriksson, Phys. Rev. B **63**, 144409 (2001).

[33] V. I. Anisimov, I. V. Solovyev, M. A. Korotin, M. T. Czyzyk, and G. A. Sawatzky, Phys. Rev. B **48**, 16929 (1993).
[34] A. I. Liechtenstein, V. I. Anisimov, and J. Zaanen, Phys. Rev. B **52**, R5467 (1995).
[35] C. E. Patrick and J. B. Staunton, Phys. Rev. B **97**, 224415 (2018).
[36] A. Landa, P. Soderlind, D. Parker, D. Aberg, V. Lordi, A. Perron, P. E. A. Turchi, R. K. Chouhan, D. Paudyal, and T. A. Lograsso, J. Alloys Compd. **765**, 659 (2018).
[37] T. Kotani, M. van Schilfgaarde, and S. V. Faleev, Phys. Rev. B **76**, 165106 (2007).
[38] J. Sinova, T. Jungwirth, J. Kucera, and A. H. MacDonald, Phys. Rev. B **67**, 235203 (2003).
[39] Y. G. Yao, L. Kleinman, A. H. MacDonald, J. Sinova, T. Jungwirth, D. S. Wang, E. G. Wang, and Q. Niu, Phys. Rev. Lett. **92**, 037204 (2004).
[40] S. Minami, F. Ishii, M. Hirayama, T. Nomoto, T. Koretsune, and R. Arita, Phys. Rev. B **102**, 205128 (2020).
[41] M. Kawamura, Comput. Phys. Commun. **239**, 197 (2019).

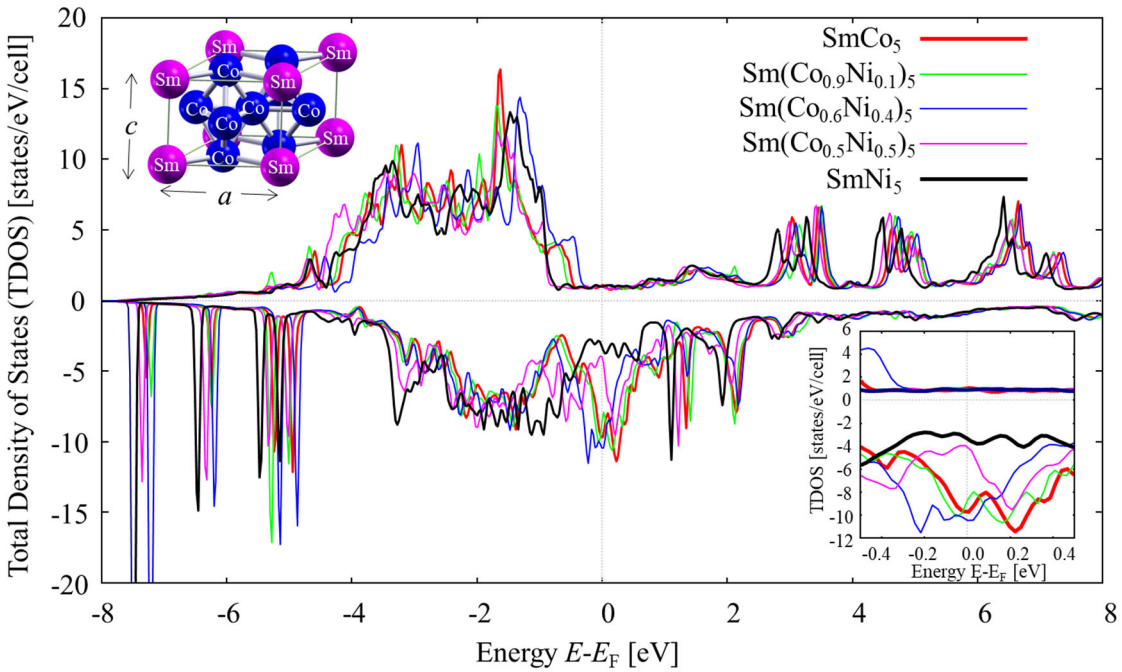

Fig. 1 Total density of sates (TDOS) of Sm(Co$_{1-x}$Ni$_x$)$_5$ (x=0, 0.1, 0.4, 0.5, and 1.0) as a function of energy relative to the Fermi energy. The positive (negative) TDOS indicates the majority (minority) spin states. (Left upper part) Schematic view graph of atomic structure of SmCo$_5$. (Right lower part) Magnification of TDOS around the Fermi energy.

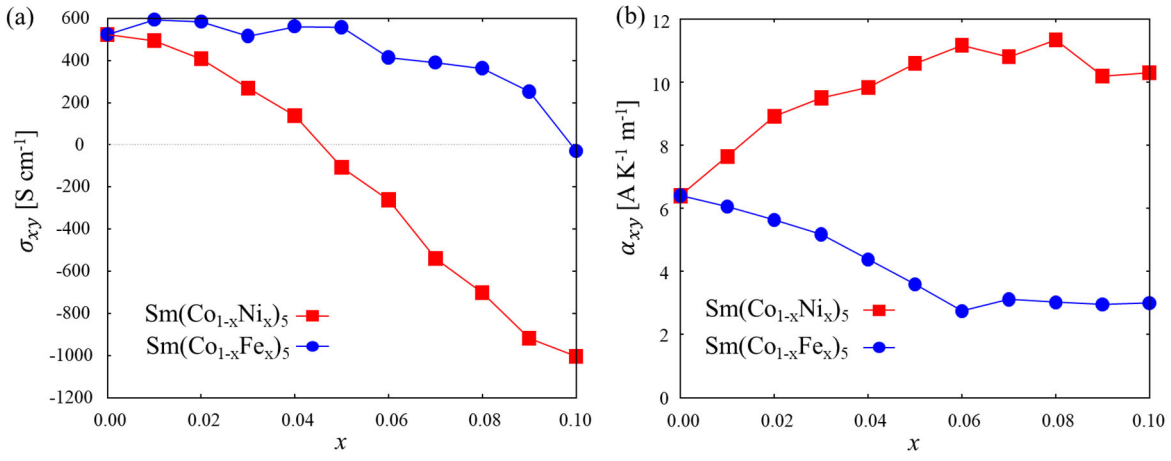

Fig.2 (a),(b) The anomalous Hall conductivity σ_{xy} and Nernst coefficient α_{xy} as a function of x in $Sm(Co_{1-x}Ni_x)_5$ and $Sm(Co_{1-x}Fe_x)_5$.

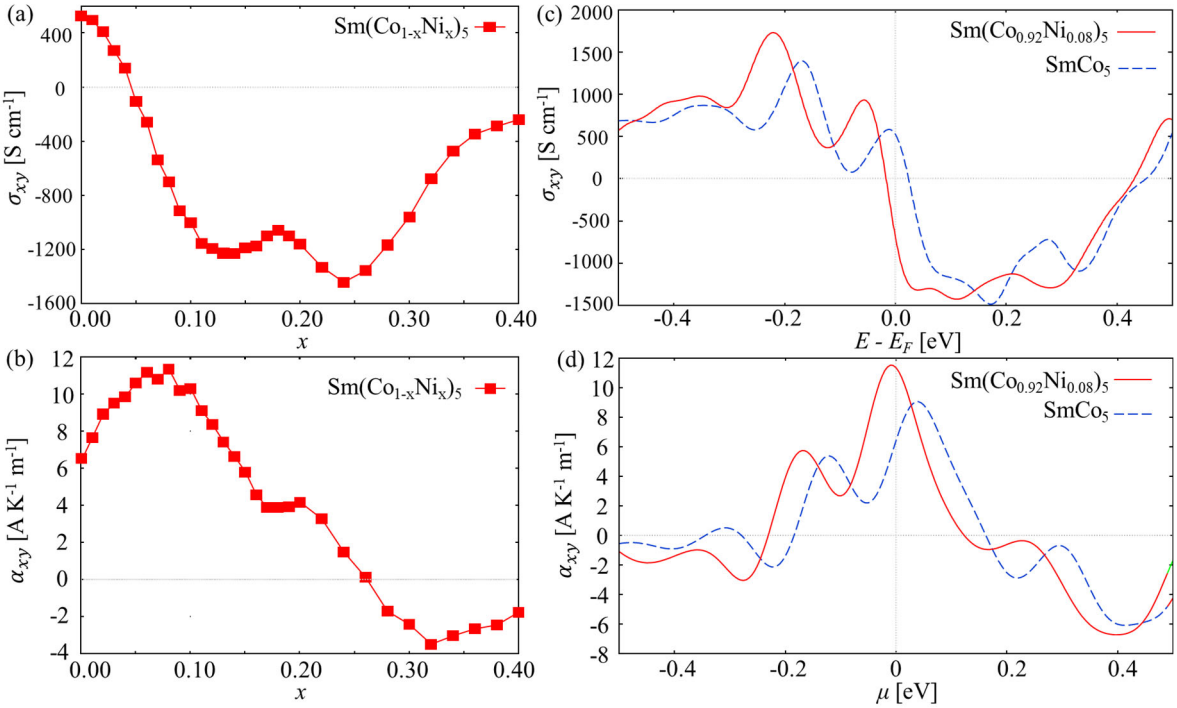

Fig. 3 (a), (b) The Ni ratio dependence of anomalous Hall conductivity and Nernst coefficient as a function of x in $Sm(Co_{1-x}Ni_x)_5$. (c) The energy E dependence of σ_{xy} for $SmCo_5$ and $Sm(Co_{0.92}Ni_{0.08})_5$. (d) The chemical potential μ dependence of α_{xy} for $SmCo_5$ and $Sm(Co_{0.92}Ni_{0.08})_5$.

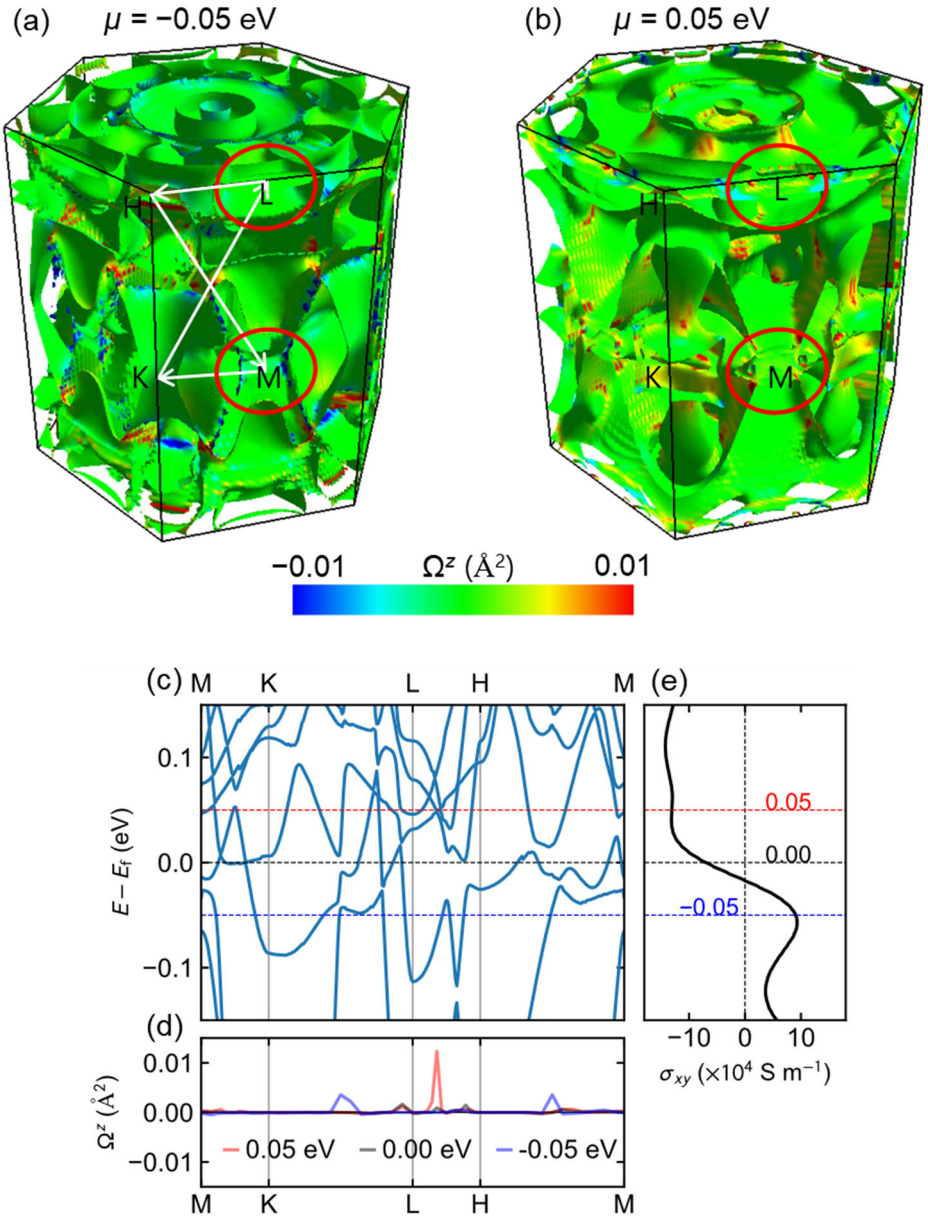

Fig. 4 (a), (b) Color map of the Berry curvatures $\Omega^z(\mathbf{k}, E)$ at (a) E = -0.05 eV and (b) E = +0.05 eV plotted on the iso-energy surface in the three-dimensional first Brillouin zone of $Sm(Co_{0.92}Ni_{0.08})_5$, which were visualized with FERMISURFER.[41] (c) The band dispersion of $Sm(Co_{0.92}Ni_{0.08})_5$ along the high-symmetry line showing large $\Omega^z(\mathbf{k}, E)$ at $E = \pm 0.05$. (d) The Berry curvatures $\Omega^z(\mathbf{k}, E)$ at $E = \pm 0.05$ along the corresponding high-symmetry line. (e) The energy dependence of σ_{xy} near the Fermi level.

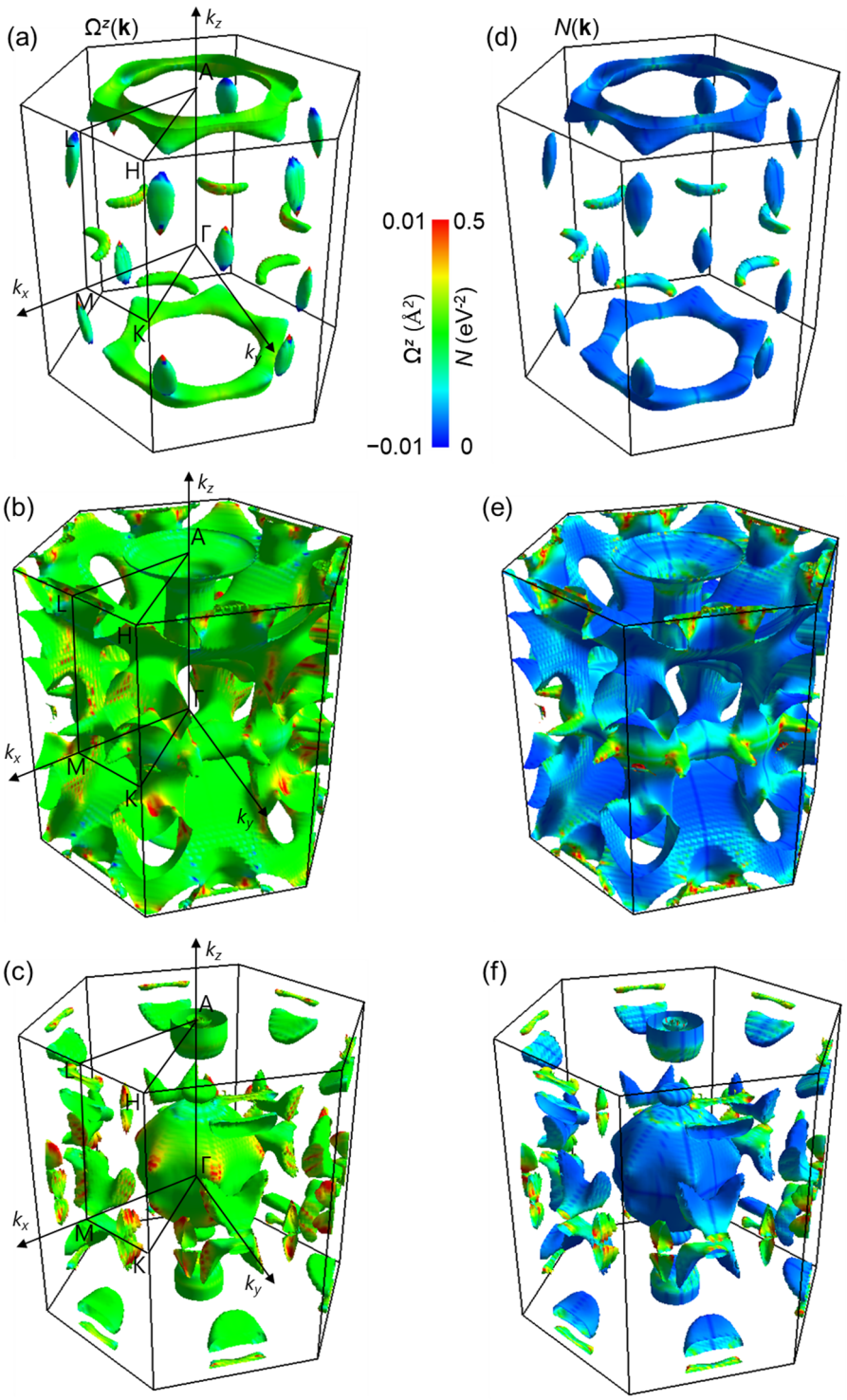

Fig. 5 (a)-(c) The mapping of the Berry curvature $\Omega^z(\mathbf{k}, E)$ onto the Fermi surface for three bands crossing the Fermi energy, respectively. (d)-(f) The mapping of the nodal line $N(\mathbf{k}, E)$ onto the Fermi surface for three bands crossing the Fermi energy, respectively. Visualizations were performed with FERMISURFER.[41]